

5f→5f transitions of U⁴⁺ ions in high-field, octahedral fluoride coordination: The Cs₂GeF₆:U⁴⁺ crystal

Belén Ordejón

Departamento de Química, C-XIV, Universidad Autónoma de Madrid, 28049 Madrid, Spain

Luis Seijo and Zoila Barandiarán^{a)}

Departamento de Química, C-XIV, Universidad Autónoma de Madrid, 28049 Madrid, Spain

and Instituto Universitario de Ciencia de Materiales Nicolás Cabrera, Universidad Autónoma de Madrid, 28049 Madrid, Spain

(Received 21 July 2005; accepted 21 September 2005; published online 18 November 2005)

The U–F bond length, totally symmetric vibrational frequency, and 5f² energy levels of the Cs₂GeF₆:U⁴⁺ crystal are predicted through quantum-chemical calculations on the embedded (UF₆)²⁻ cluster. The U⁴⁺ ions substitute for much smaller Ge⁴⁺ retaining octahedral site symmetry, which is useful to interpret the electronic transitions. The structure of the 5f² manifold: its energy range, the crystal splitting of the 5f² levels, their parentage with free-ion levels, and the energy gaps appearing within the manifold, is presented and discussed, which allows to suggest which are the possible 5f² luminescent levels. The effects of Cl-to-F chemical substitution are discussed by comparison with isostructural Cs₂ZrCl₆:U⁴⁺. The energy range of the 5f² manifold increases by some 6000 cm⁻¹ and all levels shift to higher energies, but the shift is not uniform, so that noticeable changes of order are observed from Cs₂ZrCl₆:U⁴⁺ to Cs₂GeF₆:U⁴⁺. The comparison also reveals that the green-to-blue up-conversion luminescence, which has been experimentally detected and theoretically discussed on Cs₂ZrCl₆:U⁴⁺, is quenched in the fluoride host. The results of the Cs₂GeF₆:U⁴⁺ are used as a high-symmetry model to try to understand why efficient radiative cascade emissions in the visible do not occur for charged U⁴⁺ defects in low-symmetry YF₃ crystals. The results presented here suggest that theoretical and experimental investigations of 4f/5f ions doped in octahedral, high-symmetry fluoride crystals may be conducted even when the mismatch of ionic radii between the lanthanide/actinide ions and the substituted cations of the host is considerably large. Investigations of these new materials should reveal interesting spectroscopic features without the difficulties associated with more commonly used low-symmetry fluoride hosts. © 2005 American Institute of Physics. [DOI: 10.1063/1.2121567]

I. INTRODUCTION

The interest of investigating U⁴⁺ in fluoride hosts has been stressed recently by different authors.^{1–4} It is related, on the one hand, to the wide transparency window of the fluorides that allows for very high-energy excitation and, on the other hand, to the potentiality of U⁴⁺-doped fluorides as either tunable UV solid-state lasers or as phosphor systems based on quantum cutting or cascade luminescence in the visible range.^{1–4} When the highest 5f²-¹S₀ level of U⁴⁺ defects is immersed in the 5f¹ 6d¹ band and the lowest 5f¹ 6d¹ level is well separated from the rest of lower f² states, strong, broad, and fast UV 5f¹ 6d¹ → 5f² luminescence may be observed after high-energy excitation,^{1,3} whereas if the 5f²-¹S₀ level is lower in energy and close to the 5f¹ 6d¹ band, nonradiative decay to the ¹S₀ may occur and be followed by a number of ¹S₀ emissions (in the visible range) that may be followed, on a second step, by a series of lower-frequency emissions (also in the visible) from lower f² levels.³ Whether one or the other occurs depends on the relative position of

the 5f² and 5f¹ 6d¹ manifolds, but also on the energy range of both manifolds and the number and size of energy gaps appearing between the numerous excited states, all of which result from the interplay of host effects and spin-orbit coupling on the U⁴⁺ free-ion levels and are controlled by the choice of host crystal. Fluoride crystals can affect this interplay very strongly: In effect, fluoride ligands are expected to produce smaller reductions of the energy of free-ion 5f¹ 6d¹ levels with respect to the 5f² ground state than the more polarizable chloride or bromide ligands, which may result in higher-energy 5f¹ 6d¹ crystal levels.^{5–7} They are also known to induce stronger electrostatic field than chlorides and bromides which definitely affects the structure of the 5f¹ 6d¹ manifold and also of the 5f² manifold.^{8,9} Vibrational frequencies of fluoride complexes are much higher due to the fluorine small mass, which favors nonradiative decay. Furthermore, it has been recently shown that different combinations of these features, through the choice of different fluoride hosts, may result in strong and fast 5f¹ 6d¹ → 5f² emission, such as in LiYF₄:U⁴⁺,^{1,3} or slow 5f² → 5f² luminescence, such as in YF₃:U⁴⁺.⁴ However, the fluoride hosts studied so far, of which LiYF₄ and YF₃ are good examples, accommodate the U⁴⁺ impurities in low-symmetry sites and

^{a)} Author to whom correspondence should be addressed. Electronic mail: zoila.barandiaran@uam.es

lead to charged defects, all of which make it very difficult to get detailed descriptions of the defects actually formed and of their electronic structure. So, the lack of inversion center at the substitutional site allows for $5f^2-5f^1 6d^1$ configuration mixing. Also, the need for charge compensation leads to several U^{4+} defects whose luminescence properties sum up into a complex emission spectra. In effect, variation of temperature has revealed the existence of two different crystallographic sites in $YLiF_4$ and YF_3 hosts, which differ in the way U^{4+} excess charge is compensated; the emission of these two sites sums up and leads to two groups of $5f^1 6d^1 \rightarrow 5f^2$ emissions in $LiYF_4:U^{4+}$ and to $5f^2 \rightarrow 5f^2$ and $5f^1 6d^1 \rightarrow 5f^2$ emissions in $YF_3:U^{4+}$.⁴

Taking all this into account, the study of U^{4+} defects in highly symmetric (in particular, centrosymmetric) fluoride hosts is timely and interesting because of two reasons: (i) their potentiality as either UV solid-state lasers or as quantum cutters in the visible and (ii) their use as highly symmetric models for more complex, low-symmetry U^{4+} -doped fluorides, such as those referred above. Consequently, we have decided to study the structure and $5f^2 \rightarrow 5f^2$ and $5f^2 \rightarrow 5f^1 6d^1$ transitions of U^{4+} defects in cubic Cs_2GeF_6 host using quantum-chemical methods that, making explicit use of wave functions, incorporate electron correlation, relativistic effects including spin-orbit coupling, and host embedding effects in $Cs_2GeF_6:(UF_6)^{2-}$ embedded-cluster calculations, which are similar to the ones performed on U^{3+} and U^{4+} defects in the Cs_2NaYCl_6 and Cs_2ZrCl_6 hosts.^{10,11} The cubic Cs_2GeF_6 crystal has been used to dope tetravalent transition-metal ions such as Mn^{4+} ,¹² Os^{4+} ,¹³ and Pt^{4+} ,¹⁴ and it is known to provoke strong octahedral field effects on their $d-d$ spectra. Therefore, it is a good candidate host to study neutral defects of U^{4+} ions in high-field, octahedral fluoride coordination. The mismatch between the U^{4+} and Ge^{4+} ionic radii in sixfold coordination is large (it is estimated to be about 0.44 Å),^{15,16} however, in this crystal, consecutive GeF_6 units are separated 9.021 Å from each other in the (100) directions, which allows for the necessary outwards distortion of the fluorines of the $(UF_6)^{2-}$ defect.

In this paper we present and discuss in detail the structure of the $5f^2$ manifold: its energy range, the crystal splitting of the $5f^2$ levels, their parentage with free-ion levels, and the energy gaps appearing within the manifold, all of which allow to suggest what are the possible $5f^2$ luminescent levels. We also discuss here the effects of Cl-to-F chemical substitution on the $5f^2$ manifold by comparison with previous measurements and calculations on $Cs_2ZrCl_6:U^{4+}$. In particular, these effects allow to predict that the green-to-blue up-conversion observed in Cs_2ZrCl_6 should not occur in the fluoride host. The results of the high-symmetry, high-field $Cs_2GeF_6:U^{4+}$ model are used to try to understand why radiative cascade transitions with high enough efficiency do not occur for U^{4+} in YF_3 host. The electronic structure of the $5f^1 6d^1$ manifold will be presented and analyzed in a forthcoming paper;¹⁷ the results show that the $5f^2-^1S_0$ level is immersed in the $5f^1 6d(t_{2g})^1$ band which rules out $Cs_2GeF_6:U^{4+}$ as a phosphor material based on cascade emission initiating in the $5f^2-^1S_0$ state.

II. METHOD AND DETAILS OF THE CALCULATIONS

The local structure and electronic transitions of the U^{4+} defects in Cs_2GeF_6 have been studied using the relativistic *ab initio* model potential (AIMP) embedded-cluster method.^{18,19} The method allows to partition the crystal into the $(UF_6)^{2-}$ defect cluster and its environment, the remaining host ions. Within the cluster, valence-electron correlation and relativistic effects, including spin-orbit coupling, are considered. The classical and quantum-mechanical effects of the host ions are incorporated in the cluster Hamiltonian through full ion effective one-electron operators that constitute the AIMP embedding. More detailed descriptions of the method as applied to f element ions in ionic crystals, including justifications for the choice of basis sets, active spaces, reduction of spin-orbit operators, and modification of shifting parameters referred below, can be found in Refs. 10 and 20 where U^{3+} and U^{4+} defects in chloride hosts were studied. Comparisons of the results of the method with available experimental data that serve to support its application to this new system can also be found in Refs. 10 and 20. The details corresponding to its application to the $(UF_6)^{2-}$ defect cluster and to the Cs_2GeF_6 embedding host are given next in this section.

The embedding potentials which represent the Cs_2GeF_6 ions external to the $(UF_6)^{2-}$ cluster in the $Cs_2GeF_6:(UF_6)^{2-}$ calculations presented here were obtained in a previous study of the structure and spectroscopy of Mn^{4+} defects in Cs_2GeF_6 .²¹ They accurately reproduce the quantum-mechanical interactions between the (frozen) Hartree-Fock descriptions of the external crystal ions (e.g., Cs^+ , Ge^{4+} , and F^- in Cs_2GeF_6) and the (multiconfigurational) wave functions associated with the point defect cluster $(UF_6)^{2-}$. They include (i) a long-range Coulomb term, which in ionic crystals is the corresponding Madelung potential, (ii) a short-range Coulomb term, which corrects the latter taking into account that the lattice ions are not point charges but charge densities associated with Hartree Fock wave functions, (iii) an exchange term, which stems from the fact that the generalized antisymmetric product of the cluster and the external ion wave functions fulfil the first-principles requirement of antisymmetry with respect to interchange of electrons between the cluster and lattice group functions, and (iv) a projection term, which guarantees that the defect cluster and external ion wave functions are built using linearly independent sets of orbitals; this term actually prevents variational collapse of the cluster wave functions on the lattice ions. Embedding AIMP were used for all external ions located within a cube of length $2a_0$ ($a_0=9.021$ Å for Cs_2GeF_6)²² centered on the impurity site. The ions located between this cube and a concentric one of length $4a_0$ were represented as (formal or fractional, if at the borders of the cube) point charges.

Within the $(UF_6)^{2-}$ cluster, relativistic core AIMP were used to represent the $[Xe,4f]$ core of U (Ref. 23) and the $[He]$ cores of F.²⁴ The corresponding U valence basis set ($14s10p12d9f$),²³ supplemented with three g -type functions that give maximum radial overlap with the $5f$ atomic orbital, was used and contracted as $[6s5p6d4f1g]$. In the case of F,

the valence basis set used (5s6p1d)[3s4p1d] (Ref. 24) includes one *p*-type diffuse function for anions²⁵ and one *d*-type polarization function.²⁶ Electron correlation and spin-orbit coupling were combined together as follows: In a first, spin-orbit free step, state-average complete active space self-consistent field calculations²⁷ (SA-CASSCF) were done using the relativistic Wood-Boring AIMP (Refs. 28) embedded cluster Hamiltonian omitting the spin-orbit operators [cf. Eq. (1) in Ref. 10]. These calculations account for scalar relativistic effects and nondynamic electron correlation within the 5f² manifold. The active space results from distributing the two open-shell electrons in 13 active molecular orbitals with main character U 5f, 6d, 7s; it will be referred to as CASSCF(5f,6d,7s).¹⁰ Dynamic electron correlation was taken into account using the SA-CASSCF wave functions in subsequent multistate second-order perturbation theory calculations (MS-CASPT2),^{29–32} where 68 valence electrons occupying the cluster molecular orbitals of main character F 2s, 2p, and U 5d, 6s, 6p, and 5f/6d were correlated; these calculations will be referred to as MS-CASPT2(F48,U20). In a second, spin-dependent step, we performed double-group spin-orbit configuration-interaction (CI) calculations using the whole Wood-Boring AIMP Hamiltonian.^{10,28} The shifting operator included in this Hamiltonian, the so-called spin-free-state-shifting (sfss) operator,³³ transports the dynamic electron correlation effects retrieved at the spin-orbit free MS-CASPT2(F48,U20) level onto the smaller configurational space used in the spin-orbit CI calculations, which includes the CAS(5f,6d,7s) plus all single excitations to the virtual molecular orbitals. For these calculations the bases described above were truncated to U [6s5p6d4f], F [3s4p].

The errors associated with the Wood-Boring spin-orbit operator and with the level of valence-electron correlation used can be analyzed by comparing the computed and measured 5f² → 5f² spectra of the free ion, U⁴⁺ in this case. Since these errors are expected to propagate onto the embedded-cluster calculations, this analysis allows to introduce empirical corrections to the Wood-Boring spin-orbit operator and to the spin-free-state-shifting operator to be used in the embedded-cluster calculations. This type of analysis was done on the calculated 5f² → 5f² spectrum of U⁴⁺ free ion and the corresponding empirical corrections were introduced in the calculations of U⁴⁺ defects in Cs₂ZrCl₆.²⁰ It was shown that the one-electron Wood-Boring spin-orbit operator overestimates the spin-orbit splittings by some 10%; it was also shown that the highest 5f² ³P and ¹I terms of U⁴⁺ free ion were calculated some 1000 cm⁻¹ too high compared to experiments.²⁰ In consequence, the spin-orbit operator of U [see details of this operator in Refs. 19 and 20, Eq. (3)],

$$\hat{h}_{\text{SO}}^I(i) = \lambda^I \sum_{n\ell \in \text{valence}} V_{\text{SO},n\ell}^{\text{I,MP}}(r_i) \hat{O}_i^I \hat{t}_i^I \hat{O}_i^I \quad (1)$$

(with *I*=U), was scaled by a factor of λ^U=0.9 in the embedded-cluster calculations. The δ(*i*Γ) parameters of the spin-free-state-shifting operator [see details of this operator in Refs. 19 and 20, Eqs. (1) and (2)],

$$\sum_{iSM_S\Gamma\gamma} \delta(i\Gamma) |\Phi^{\mathcal{P}}(iSM_S\Gamma\gamma)\rangle \langle \Phi^{\mathcal{P}}(iSM_S\Gamma\gamma)|, \quad (2)$$

that are defined as

$$\delta(i\Gamma) = [E^{\mathcal{G}}(i\Gamma) - E^{\mathcal{G}}(1^3T_{1g})] - [E^{\mathcal{P}}(i\Gamma) - E^{\mathcal{P}}(1^3T_{1g})], \quad (3)$$

that is, the difference between the MS-CASPT2 transition energies (first term in square parentheses) and the CASSCF(5f,6d,7s)+singles transition energies from the 1³T_{1g} ground state (second term in square parentheses),^{19,20} were substituted by δ'(*i*Γ)=[δ(*i*Γ)−1000] cm⁻¹ for those *i*Γ terms emparented with the free-ion ³P and ¹I, that is, 4³T_{1g}(³P), and 2¹A_{1g}, 1¹A_{2g}, 3¹E_g, 2¹T_{1g}, 3¹T_{2g}, and 4¹T_{2g}(¹I). In this work, we also scaled the U spin-orbit operator by a factor λ^U=0.9. Analogously, we added −1000 cm⁻¹ correction to the embedded-cluster terms related to the free-ion ³P and ¹I. However, due to the fact that the mixture of free-ion terms is larger in the higher-field fluoride than in the chloride host, we decided to establish the correspondence between free-ion and embedded-cluster terms and to weight the correction, in accord with the results of a projection of the embedded-cluster 5f² wave functions Φ^{(UF₆)²⁻}(*i*SM_SΓγ) on the 5f² free-ion space {Φ^{U⁴⁺}(*j*SM_SLM_L)}, as follows:

$$\begin{aligned} & \Phi_{\text{os}}^{(\text{UF}_6)^{2-}}(iSM_S\Gamma\gamma) \\ &= \sum_{jLM_L} |\Phi_{\text{os}}^{\text{U}^{4+}}(jSM_SLM_L)\rangle \\ & \quad \times \langle \Phi_{\text{os}}^{\text{U}^{4+}}(jSM_SLM_L) | \Phi_{\text{os}}^{(\text{UF}_6)^{2-}}(iSM_S\Gamma\gamma) \rangle \\ & \quad + \text{residue}. \end{aligned} \quad (4)$$

As indicated with the subscript os, the projection and, therefore, the overlaps in Eq. (4) were calculated integrating only the open-shell parts of the SA-CASSCF wave functions Φ^{U⁴⁺}(*j*SM_SLM_L) and Φ^{(UF₆)²⁻}(*i*SM_SΓγ), which have the same number of electrons; for this purpose, the same molecular basis set (described above) was used for the free-ion than for the embedded-cluster wave functions, and the cluster wave functions used were calculated at 2.17 Å U–F internuclear distance. The free-ion ³P, ¹I, or, in general, *j*SL contributions to the *i*Γ embedded-cluster terms were then estimated as

$$w(jSL, i\Gamma) = \sum_{M_L} \langle \Phi_{\text{os}}^{\text{U}^{4+}}(jSM_SLM_L) | \Phi_{\text{os}}^{(\text{UF}_6)^{2-}}(iSM_S\Gamma\gamma) \rangle^2 \quad (5)$$

and were used to weight the −1000 cm⁻¹ empirical corrections associated with ³P and ¹I as

$$\begin{aligned} \delta'(i\Gamma) &= \{\delta(i\Gamma) - [w(^3P, i\Gamma) + w(^1I, i\Gamma)] \\ & \quad \times 1000\} \text{ cm}^{-1}, \end{aligned} \quad (6)$$

where the δ'(*i*Γ) are the new corrected parameters of the spin-free-state-shifting operators of Eq. (2). The values of the w(*j*SL, *i*Γ) components for all embedded-cluster terms are presented in Table I; they show the considerable mixture of free-ion terms in the spin-free 5f² cluster wave functions.

TABLE I. Analysis of spin-orbit free $5f^2$ embedded-cluster wave functions $\Phi^{(\text{UF}_6)^{2-}}(iS\Gamma)$ in terms of $5f^2$ free-ion wave functions $\Phi^{U^{4+}}(jSL)$. The tabulated values correspond to $w(jSL, iS\Gamma)$ in Eq. (5); they have been calculated at 2.17 Å U–F distance. See text for details.

Free-ion jSL terms	Embedded-cluster $iS\Gamma$ terms							
	1^3T_{1g}	2^3T_{1g}	1^3T_{2g}	1^3E_g	2^3T_{2g}	1^3A_{2g}	3^3T_{1g}	4^3T_{1g}
3H	0.81	0.77	0.43	0.91	0.50		0.20	0.07
3F	0.07	0.17	0.48		0.44	0.91	0.59	0.10
3P							0.14	0.78
residue	0.12	0.05	0.09	0.09	0.07	0.09	0.08	0.05
	1^1T_{1g}	1^1A_{1g}	1^1E_g	1^1T_{2g}	2^1T_{2g}	2^1E_g	2^1A_{1g}	2^1T_{1g}
1G	0.79	0.58	0.90	0.87		0.03	0.22	0.15
1D			0.02		0.13	0.84		
1I	0.12	0.31		0.01	0.76	0.03	0.54	0.82
1S							0.19	
residue	0.09	0.11	0.07	0.12	0.11	0.11	0.05	0.04
	3^1T_{2g}	1^1A_{2g}	4^1T_{2g}	3^1E_g	3^1A_{1g}			
1G			0.01		0.13			
1D	0.51		0.29	0.02				
1I	0.44	0.90	0.63	0.86	0.10			
1S					0.72			
residue	0.05	0.10	0.08	0.12	0.05			

The small values of the residues indicate the notably localized nature of the manifold.

We calculated the potential-energy surfaces of all 40 $5f^2$ spin-orbit levels of $\text{Cs}_2\text{GeF}_6:(\text{UF}_6)^{2-}$ using the methods we have just described. We obtained the U–F equilibrium distances R_e and totally symmetric harmonic vibrational frequencies $\bar{\nu}_{a_{1g}}$ from the potential-energy surfaces as in Ref. 34. The minimum-to-minimum transition energies T_e which should be very close to zero-phonon transitions were also calculated. All these results are presented in Table II and are discussed in the next section. The analysis of the embedded-cluster spin-orbit wave functions in terms of spin-orbit free wave functions is presented in Table II for $R(\text{U–F}) = 4.10$ a.u. = 2.17 Å. This, together with the results in Table I and the analyses of the U^{4+} free-ion spin-orbit wave functions in terms of the free-ion terms presented in Ref. 20, allows to find out the parentage of crystal levels with free-ion levels.

The calculations were done using the MOLCAS program system³⁵ and a modified version of the COLUMBUS package.³⁶ All AIMP data (for embedding and/or for cores) and valence basis sets can be found in Ref. 37.

III. RESULTS AND DISCUSSION

The main features of the electronic structure of the $5f^2$ manifold, whose spectroscopic constants appear in Table II, are discussed in this section paying particular attention to the following aspects: An overall description of the $5f^2$ manifold of $\text{Cs}_2\text{GeF}_6:U^{4+}$ is given in Sec. III A which includes a discussion on what are the possible luminescent levels. The large changes on the $5f^2$ manifold due to chlorine-to-fluorine chemical substitution are discussed in Sec. III B, where previous theoretical and experimental results on $(\text{UX}_6)^{2-}(\text{X}$

= F, Cl) are also used.^{8,9} The green-to-blue up-conversion luminescence, observed in $\text{Cs}_2\text{ZrCl}_6:U^{4+}$,^{38,39} is predicted to be quenched in the fluoride host, as described in Sec. III C. And finally, the results of the high-symmetry model $\text{Cs}_2\text{GeF}_6:U^{4+}$ are used in Sec. III D to help understand the quenching of the second step in photon cascade emission in $\text{YF}_3:U^{4+}$.

A. The electronic structure of the $5f^2$ manifold of $\text{Cs}_2\text{GeF}_6:U^{4+}$: Luminescent levels

The $5f^2$ manifold is formed by parallel potential-energy surfaces whose U–F bond lengths average to 2.174 ± 0.005 Å and a_{1g} vibrational frequencies to 563 ± 6 cm^{−1} (see Table II). The effects of the large crystal field on the U^{4+} 3H_4 ground state can be directly seen in Table II; they lead to the ground, $1A_{1g}$, and excited, $1T_{1g}$, $1E_g$, and $1T_{2g}$, crystal components and amount to 4300 cm^{−1} total splitting. They are also responsible for a large mixture of higher U^{4+} energy levels in the remaining crystal components, which results in the loss of the large energy gaps existing in the free ion (4200 cm^{−1} between 3H_4 and 3F_2 and 4900 cm^{−1} between 3H_6 and 1D_2),^{40,41} on the one hand, and the difficulty to associate crystal levels to U^{4+} levels, on the other hand, as shown by the labels that indicate the free-ion term parentage in Table II. In effect, Table I shows the large mixing of free-ion terms in some spin-orbit free states such as 1^3T_{2g} , 2^3T_{2g} , 3^3T_{1g} , 1^1A_{1g} , 2^1A_{1g} , 3^1T_{2g} , and 4^1T_{2g} . The mixing is wider at the spin-orbit level and, as a result, the correspondence between crystal levels and free-ion levels is extremely limited. As a consequence, all states except the highest $7A_{1g}(^1S_0)$ form a dense set of close lying states below 32 000 cm^{−1} with some small energy gaps of 1000–1700 cm^{−1} (indicated in Table II by single horizontal lines) and only three significant energy

TABLE II. Results of sfss spin-orbit Wood-Boring-AIMP (UF₆)²⁻ embedded-cluster calculations that include Cs₂GeF₆ embedding, 68 valence-electron correlation, and relativistic effects, including spin-orbit coupling. U–F bond distances R_e , in Å, totally symmetric vibrational frequencies $\bar{\nu}_{a_{1g}}$, in cm⁻¹, minimum-to-minimum energy differences T_e , in cm⁻¹, and analyses of the spin-orbit wave functions of Cs₂GeF₆:(UF₆)²⁻ are listed. Manifold averages (indicated by $\langle 5f^2 \rangle$) and root-mean-square deviations of the equilibrium distances R_e and breathing mode vibrational frequencies $\bar{\nu}_{a_{1g}}$ are also given.

State	R_e	$\bar{\nu}_{a_{1g}}$	T_e^a	Weights of spin-orbit free wave functions larger than 15% ^b						
$\langle 5f_2 \rangle$	2.174±0.005	563±6								
From 3H_4										
1A _{1g}	2.165	564	0	(91.83)	90.4	1 $^3T_{1g}$				
1T _{1g}	2.168	563	1755	(90.14)	62.75	1 $^3T_{1g}$	19.11	1 $^3T_{2g}$		
1E _g	2.170	559	2558	(87.58)	34.11	1 $^3T_{2g}$	27.50	2 $^3T_{1g}$	25.12	1 $^3T_{1g}$
1T _{2g}	2.172	555	4262	(92.05)	69.65	2 $^3T_{1g}$				
From 3F_2 , 3H_5 , 3F_3 , 3F_4 , and 3H_6										
2E _g	2.171	566	6 776	(95.58)	55.63	2 $^3T_{1g}$				
2T _{2g}	2.168	564	6 923	(92.74)	55.25	1 $^3T_{1g}$	15.63	1 3E_g		
2T _{1g}	2.168	556	7 836	(82.48)	37.08	1 $^3T_{1g}$	31.49	1 $^3T_{2g}$	17.49	1 $^1T_{1g}$
3T _{1g}	2.170	571	8 761	(96.21)	63.89	2 $^3T_{1g}$	30.84	1 $^3T_{2g}$		
3T _{2g}	2.177	565	9 475	(84.08)	32.54	2 $^3T_{2g}$	17.47	1 $^3T_{1g}$	16.03	3 $^3T_{1g}$
2A _{1g}	2.164	563	9 744	(63.66)	60.10	2 $^3T_{1g}$	36.19	1 $^1A_{1g}$		
3E _g	2.174	554	10 665	(73.01)	38.56	2 $^3T_{2g}$	24.18	1 1E_g	17.66	1 $^3T_{1g}$
4E _g	2.168	567	12 038	(91.37)	47.39	1 $^3T_{2g}$	40.67	1 $^3T_{1g}$		
4T _{2g}	2.172	562	12 069	(76.18)	27.41	1 $^3T_{2g}$	23.60	1 $^1T_{2g}$	17.52	2 $^3T_{2g}$ 16.41 2 $^3T_{1g}$
4T _{1g}	2.174	560	12 249	(62.46)	38.72	2 $^3T_{2g}$	37.49	1 $^1T_{1g}$	17.41	1 3E_g
1A _{2g}	2.174	561	12 325	(99.38)	76.53	2 $^3T_{2g}$	22.85	1 $^3T_{2g}$		
5T _{2g}	2.172	567	13 336	(92.08)	42.76	1 $^3T_{2g}$	22.11	1 $^3T_{1g}$		
5T _{1g}	2.178	562	13 501	(98.56)	50.29	1 3E_g	29.80	2 $^3T_{2g}$		
5E _g	2.179	559	14 245	(59.52)	45.26	3 $^3T_{1g}$	34.13	1 1E_g		
2A _{2g}	2.175	565	14 811	(95.90)	72.64	1 $^3T_{2g}$	23.26	2 $^3T_{2g}$		
6T _{2g}	2.178	559	15 052	(77.50)	46.56	1 $^3A_{2g}$	21.19	1 $^1T_{2g}$	15.07	1 3E_g
3A _{1g}	2.166	545	15 552	(48.08)	51.18	1 $^1A_{1g}$	37.53	2 $^3T_{1g}$		
6T _{1g}	2.175	556	16 669	(75.05)	22.57	1 $^1T_{1g}$	21.33	2 $^3T_{2g}$	20.77	2 $^3T_{1g}$
7T _{2g}	2.179	552	17 246	(82.63)	30.30	3 $^3T_{1g}$	25.37	1 3E_g		
From 1D_2 , 1G_4 , 3P_0 , 3P_1 , 1I_6 , and 3P_2										
8T _{2g}	2.173	572	18 660	(44.24)	48.06	2 $^1T_{2g}$				
6E _g	2.174	568	18 988	(77.98)	34.87	3 $^3T_{1g}$	34.53	2 $^3T_{2g}$	20.30	1 1E_g
4A _{1g}	2.175	567	19 052	(61.48)	53.74	3 $^3T_{1g}$	34.73	2 $^1A_{1g}$		
7T _{1g}	2.176	571	19 204	(70.38)	59.80	3 $^3T_{1g}$	22.06	2 $^1T_{1g}$		
9T _{2g}	2.172	560	20 748	(56.98)	37.92	1 $^1T_{2g}$	29.64	1 $^3A_{2g}$		
7E _g	2.177	562	21 057	(37.73)	59.49	2 1E_g	21.26	4 $^3T_{1g}$		
5A _{1g}	2.183	565	22 399	(89.31)	85.88	4 $^3T_{1g}$				
8T _{1g}	2.175	566	23 718	(41.53)	59.44	2 $^1T_{1g}$	22.86	4 $^3T_{1g}$		
6A _{1g}	2.175	567	23 905	(39.62)	59.50	2 $^1A_{1g}$	38.30	3 $^3T_{1g}$		
10T _{2g}	2.172	568	24 252	(13.70)	85.53	3 $^1T_{2g}$				
3A _{2g}	2.174	561	24 729	(4.54)	95.40	1 $^1A_{2g}$				
9T _{1g}	2.182	566	24 903	(84.00)	76.36	4 $^3T_{1g}$	15.42	2 $^1T_{1g}$		
11T _{2g}	2.178	569	27 381	(80.77)	79.21	4 $^3T_{1g}$				
8E _g	2.179	566	27 745	(61.15)	59.66	4 $^3T_{1g}$	23.43	2 1E_g		
12T _{2g}	2.185	563	31 025	(9.85)	89.31	4 $^1T_{2g}$				
9E _g	2.191	561	32 312	(15.79)	82.13	3 1E_g				
From 1S_0										
7A _{1g}	2.177	569	46 168	(6.54)	93.34	3 $^1A_{1g}$	6.44	4 $^3T_{1g}$		

^aEnergy gaps between spin-orbit states are indicated by a single (1000–1600 cm⁻¹) or a double (>2500 cm⁻¹) horizontal line.

^bWeights are given in % and correspond to calculations at $R(\text{U–F})=2.17$ Å. Total spin-triplet character is given in parentheses.

gaps (indicated in Table II by double horizontal lines), $1T_{2g}$ and $2E_g$, and $9T_{1g}$ and $11T_{2g}$ states are separated by some 2500 cm^{-1} ($=4.4\bar{\nu}_{a_{1g}}$) and $8E_g$ and $12T_{2g}$ by some 3300 cm^{-1} ($=5.9\bar{\nu}_{a_{1g}}$). A detailed experimental study of the vibronic spectra of U^{4+} in Cs_2ZrBr_6 by Flint and Tanner^{42,43} showed that multiphonon relaxation dominates the radiative process when the energy gap below the electronic level is less than four quanta of the highest-frequency phonon coupled to the lattice, i.e., 800 cm^{-1} for $(UBr_6)^{2-}$; they observed luminescence from those levels located above energy gaps of four to seven quanta. The application of this empirical rule to our results in $Cs_2GeF_6:U^{4+}$ sets the limit of smallest energy gap, that favors radiative emission, to $4\bar{\nu}_{a_{1g}}=2250\text{ cm}^{-1}$, which suggests that $12T_{2g}$, $11T_{2g}$, and $2E_g$ might be luminescent levels in this material. In addition, the results of the analyses of the spin-orbit wave functions presented in Table II show that there is a notable change on the spin-triplet character of $12T_{2g}$ (9.85) and $8E_g$ (61.15), which supports further the metastability of $12T_{2g}$ based on spin selection rules.

B. Comparison of the $5f^2$ manifolds of $Cs_2ZrCl_6:U^{4+}$ and $Cs_2GeF_6:U^{4+}$

The changes originated by the chlorine-to-fluorine chemical substitution are considerable, as it is clear from the comparison of the $5f^2$ manifolds of U^{4+} defects in isomorphous Cs_2ZrCl_6 and Cs_2GeF_6 hosts, calculated using the same methods of quantum chemistry (cf. Table II and Ref. 11, Table IV, and Fig. 1). Their local structure is very different: The bond length difference is very large, 0.43 Å ($R_e=2.605\pm0.003\text{ Å}$ for the chloride and $R_e=2.174\pm0.005\text{ Å}$ for the fluoride), and the totally symmetric vibrational frequency of the fluoride is much higher, due to the ligands smaller mass ($\bar{\nu}_{a_{1g}}=320\pm2\text{ cm}^{-1}$ for the chloride and $\bar{\nu}_{a_{1g}}=563\pm6\text{ cm}^{-1}$ for the fluoride). The effects of the chemical environment on the $U^{4+} 5f^2$ levels are also much larger in the Cs_2GeF_6 host. The total splitting of the 3H_4 free-ion level is 76% larger in the fluoride (the energy difference between $1A_{1g}$ and $1T_{2g}$ is 2428 cm^{-1} in the chloride and 4262 cm^{-1} in the fluoride) and analogous effects on the higher free-ion levels make the energy range of the $5f^2$ manifold some 6000 cm^{-1} larger in the Cs_2GeF_6 host, which can be illustrated by the following energy differences: $T_e(9E_g;Cs_2GeF_6)-T_e(9E_g;Cs_2ZrCl_6)=6000\text{ cm}^{-1}$ and $T_e[7A_{1g}(^1S_0);Cs_2GeF_6]-T_e[7A_{1g}(^1S_0);Cs_2ZrCl_6]=6300\text{ cm}^{-1}$. All levels shift to higher energies in Cs_2GeF_6 , but the shift is not uniform, so that noticeable changes of order are observed going from Cs_2ZrCl_6 to Cs_2GeF_6 . All these results agree with available experimental studies that compare hexafluoro and hexachloro complexes of tetravalent uranium in solid salts and in solution,^{8,9} as we comment next.

Experimental data on octahedral hexafluoro complexes of tetravalent uranium are very scarce. This is probably related to the fact that coordination 6 is very uncommon for fluoride complexes of tetravalent actinides, as pointed out by Ryan *et al.*,⁸ who reported the first preparation of the octahedral hexafluoro complexes $(AnF_6)^{2-}$ ($An=U,Np,Pu$) and measured their absorption spectra both in solid salts $[(C_2H_5)_4N]_2AnF_6$ and in solutions. From the comparison of

their observations in the hexafluoro complexes with previous results on octahedral hexachloro and hexabromo complexes, the authors concluded that the absorption spectra are very sensitive to the actinide chemical environment and that the differences are more marked going from F to Cl than from Cl to Br ligands. They found large shifts of the transitions to higher energies in the fluorides compared to the chlorides, which are not uniform for all levels, and result in severe change of order of transitions. They also pointed out large mixings of vibronic groups due to larger vibrational frequencies in the fluorides. As a result, few transitions in the room-temperature spectra of the $(AnF_6)^{2-}$ could be unambiguously matched to corresponding transitions in the $(AnCl_6)^{2-}$,⁸ and a detailed analysis of the $5f^2\rightarrow5f^2$ transitions was not possible.⁸

A comparative study of the low-temperature absorption spectra of $[(C_2H_5)_4N]_2UX_6$ ($X=F,Cl,Br,I$) and of Cs_2UCl_6 was reported by Wagner *et al.*⁹ a few years later. The authors concluded that the spectrum of the $[(C_2H_5)_4N]_2UF_6$ shows almost no similarity to the other $(UX)_6^{2-}$ and that the peaks are strongly shifted to higher energies. Nevertheless, for the assignments of the levels below $12\,000\text{ cm}^{-1}$ they assumed that the order of levels in the hexafluoride was the same as in the other hexahalides, whereas the assignments of levels above that threshold were determined by the proximity of the crystal-field-fitted and observed levels. Given that the measured peaks are predominately vibronic, because the $f\rightarrow f$ transitions are electric dipole forbidden in centrosymmetric sites, the missing electronic origins were deduced by assuming they are at the center of the space between two peaks resulting from the coupling of an odd vibrational mode with the ground and the excited electronic states, respectively (namely, peak 1=zero-phonon- ν_{odd} and peak 2=zero-phonon+ ν_{odd}); following this procedure, the odd vibrational mode was deduced as approximately equal to one-half the separation between peaks. With this procedure, sixteen zero-phonon lines were deduced up to $18\,051\text{ cm}^{-1}$ from the observed vibronic lines and they were used in the crystal-field fitting. The values of the odd vibrational frequencies deduced are very high (from Ref. 9, Table II: 362, 457, 596, and 661 cm^{-1}), as expected for a hexafluoride or for the combination of normal modes. The main features of their spectra and ours coincide: The peaks shift to higher energies and the $5f^2$ energy range increases going from Cl to F coordination. The results of their fitting for $[(C_2H_5)_4N]_2UF_6$ has been included in Fig. 1 where the energy levels and the overall energy range of the manifold can be compared with our results in Cs_2GeF_6 .

Finally, we would like to comment on the possible errors our minimum-to-minimum energy values T_e listed in Table II might have. We estimate them with the root-mean-square deviations of the calculated versus experimental data available given in Ref. 11 for $Cs_2ZrCl_6:U^{4+}$, which seem reasonable because the methods used for the calculations are basically the same. Consequently, we might expect increasing errors with energy in the order of¹¹ $2E_g\rightarrow7T_{2g}$: $400\text{--}700\text{ cm}^{-1}$ and $8T_{2g}\text{--}9E_g$: $1500\text{--}1700\text{ cm}^{-1}$. In all cases, the errors are overestimations.

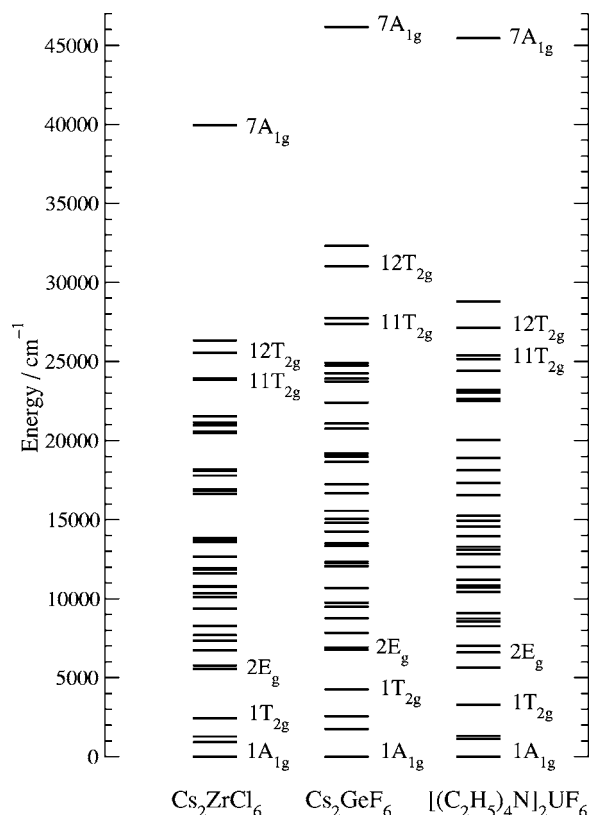


FIG. 1. $5f^2 \rightarrow 5f^2$ transition energies for Cs₂ZrCl₆:U⁴⁺ (Ref. 11), Cs₂GeF₆:U⁴⁺ (this work), and [(C₂H₅)₄N]₂UF₆ (Ref. 9).

C. Quenching of green-to-blue up-conversion luminescence in Cs₂GeF₆

Green-to-blue up-conversion luminescence was observed experimentally in U⁴⁺-doped Cs₂ZrCl₆ by Xu *et al.*³⁸ and by Tanner *et al.*³⁹ Different interpretations were given that ascribed the up-converted luminescence to either the U⁴⁺ defects³⁸ or to unavoidable UO₂²⁺ impurities in the Cs₂GeF₆:U⁴⁺ crystals.³⁹ The observations and the two apparently conflicting interpretations were conciliated by an up-conversion mechanism proposed, on the basis of quantum-chemical calculations, which pointed out the important role of the lowest-lying levels of the $5f^1 6d^1$ manifold in the up-conversion.¹¹ According to the calculations, the excitation produced by a first green photon (19 436 cm⁻¹) would be followed by nonradiative relaxation to lower energy levels, namely, $8T_{1g}$ and $8T_{2g}$, which could be the origins of an efficient, dipole-allowed second absorption of a green photon leading to $8T_{1g}/8T_{2g} \rightarrow 5f^1 6d^1$ transitions that could be followed by either nonradiative relaxation to high $5f^2$ levels of the U⁴⁺ impurity, emitting in the blue, and/or by energy transfer from the lowest $5f^1 6d^1$ state to levels of the UO₂²⁺, which, after nonradiative decay, would emit also in the blue.¹¹ Very important in this mechanism is the fact that both $8T_{2g}$ and $8T_{1g}$ are separated from the next lower-lying levels by large energy gaps of 2800 and 2300 cm⁻¹, respectively, larger than $8\bar{\nu}_{a_{1g}}$ and $7\bar{\nu}_{a_{1g}}$ ($\bar{\nu}_{a_{1g}} = 320$ cm⁻¹ in Cs₂ZrCl₆:U⁴⁺), which makes them stable enough so as to be the origins for the second green-photon absorption.

None of the important steps of the preceding mechanism that follow the first green-photon absorption should occur in

the Cs₂GeF₆:U⁴⁺ crystal, with or without UO₂²⁺ impurities present. This is due to the lack of stable energy levels that could stop the nonradiative decay and, at the same time, be the origins for efficient $5f^2 \rightarrow 5f^1 6d^1$ second green-photon absorption. In effect, given the shift of levels to higher energies, commented above, and assuming that our T_e values could be calculated some 1500 cm⁻¹ too high in the 19 436 cm⁻¹ energy region, the green absorption could excite $5f^2$ vibronic levels around the $7T_{1g}$ and $9T_{2g}$ origins, far below the first stable high energy level $11T_{2g}$ (Table II). In any case, after the first excitation and as a consequence of the lack of large energy gaps, nonradiative decay should dominate^{42,43} and should occur down to the $2E_g$ state. From this low energy level, a second green-photon absorption could only lead to low intensity, dipole-forbidden $5f^2 \rightarrow 5f^2$ excitation to $9T_{1g}$ or lower levels, which would decay again, nonradiatively, to $2E_g$ (Table II). Consequently, the pumping of states in the blue of U⁴⁺ or UO₂²⁺ through nonradiative decay or energy transfer from the lowest $5f^1 6d^1$, respectively, is not possible in the hexafluoride and up-converted blue emission should not be observed.

D. Cs₂GeF₆:U⁴⁺: A high-symmetry model to interpret photon cascade emission in YF₃:U⁴⁺

Now we can use the results of the electronic structure of Cs₂GeF₆:U⁴⁺ to try to understand the low efficiency in the second step of photon cascade emission in the low-symmetry YF₃:U⁴⁺ crystal.

Isoelectronic $4f^2$ Pr³⁺-doped fluorides have been extensively investigated in a search for new luminescent materials, useful for luminescence lamps, capable of emitting more than one photon in the visible spectral range after excitation by high-energetic Xe noble-gas discharge. This process, called photon cascade emission, quantum cascade emission, or quantum cutting, has been described in a recent overview about Pr³⁺-doped fluorides,⁴⁴ as resulting from a two-step $4f^2 \rightarrow 4f^2$ emission where $^1S_0 \rightarrow ^1I_6$ is followed by $^3P_0 \rightarrow ^3H_4$ emission after high-energetic excitation to the $4f^1 5d^1$ band, whose lowest energy level is above 1S_0 . Given that the first step ($^1S_0 \rightarrow ^1I_6$) in photon cascade emission in Pr³⁺-doped fluorides occurs in the ultraviolet spectral range, U⁴⁺-doped YF₃ has been investigated as more interesting phosphor, since this emission occurs in the visible.⁴ However, it has been found that the second step in cascade emission, $^3P_0 \rightarrow ^3H_4$, seems to be quenched, which makes the overall efficiency of quantum cutting in U⁴⁺-doped YF₃ very low.⁴ The authors have pointed out that either multiphonon relaxation or cross relaxation could be the possible loss mechanisms, but none of these have been investigated.⁴ According to the present calculations, in Cs₂GeF₆:U⁴⁺, $7A_{1g}$ is clearly related to U⁴⁺ 1S_0 and appears to be immersed in the $5f^1 6d(t_{2g})^1$ band.¹⁷ Therefore, $7A_{1g}$ cannot be a luminescent level and cascade emission, originating in it, should not be observed in this crystal.

Yet, given that the $5f^2$ manifold should be less sensitive to the fluoride host change than the $5f^1 6d^1$ manifold, the results in this high-symmetry model system should be useful to try to interpret the reasons behind the quenching of the

second step in the cascade emission observed in the YF_3 host, as we do next. As discussed in Sec. III A, the energy gaps found in Cs_2GeF_6 are, in general, very small, which favors multiphonon relaxation. In the high-energy part of the manifold, only the levels $12T_{2g}(^1I_6)$ and $11T_{2g}(^3P_2)$ are predicted to be luminescent levels. (Note that the main free-ion level is indicated in parentheses, even if this is an approximation; see Tables I and II for the corresponding associations). Below $11T_{2g}(^3P_2)$ no other metastable state is found down to $2E_g$; in particular, the crystal level which is most closely related to 3P_0 , $5A_{1g}(^3P_0)$, which should be the origin for the second-step photon cascade emission, appears to be only 1400 cm^{-1} ($=2.5\bar{\nu}_{a_{1g}}$) above the next, lower state. According to the four-quanta empirical law of Flint and Tanner^{42,43} referred above, this small energy gap makes it very likely that nonradiative decay takes place, which leads to the quenching of the second step in photon cascade emission. The same conclusions should hold if the structural differences between Cs_2GeF_6 and YF_3 are taken into account qualitatively. The higher coordination of U^{4+} in YF_3 (9) should result in an energetically shorter $5f^2$ manifold due to smaller crystal-field splitting and correspondingly smaller mixings of the energy levels; on the opposite direction, the lower site symmetry of U^{4+} in YF_3 should cause splittings and mixings of the crystal levels which are degenerate in an octahedral site. As a result, a not too different structure of energy gaps in the $5f^2$ manifold should be expected in the ninefold, low-symmetry fluoride coordination in $\text{YF}_3:\text{U}^{4+}$. In particular, too small energy gaps below $5A_{1g}(^3P_0)$ or nearby levels should be expected in the $\text{YF}_3:\text{U}^{4+}$ crystal that quench the second step of photon cascade emission.

IV. CONCLUSIONS

We present here the results of AIMP embedded-cluster calculations on $(\text{UF}_6)^{2-}$ that include Cs_2GeF_6 embedding, 68 valence-electron correlation, and relativistic effects, including spin-orbit coupling. The U–F bond length, totally symmetric vibrational frequency, and energy of the $5f^2$ levels have been calculated and show large effects of the fluoride host on the U^{4+} free-ion levels and wave functions. Only a few large energy gaps between $5f^2$ states are found and, therefore, only three states are expected to be luminescent levels below the $5f^1 6d^1$ band. The effects of Cl-to-F chemical substitution are discussed by comparison with isostructural $\text{Cs}_2\text{ZrCl}_6:\text{U}^{4+}$; they are found to be very large, the energy range of the $5f^2$ manifold increases by 6000 cm^{-1} and all levels shift to higher energies, but the shift is not uniform and noticeable changes of order are observed going from $\text{Cs}_2\text{ZrCl}_6:\text{U}^{4+}$ to $\text{Cs}_2\text{GeF}_6:\text{U}^{4+}$. The comparison allows to predict that the green-to-blue up-conversion luminescence, which has been experimentally detected and theoretically discussed on $\text{Cs}_2\text{ZrCl}_6:\text{U}^{4+}$, should be quenched in the fluoride host. $\text{Cs}_2\text{GeF}_6:\text{U}^{4+}$ is ruled out as a phosphor material based on cascade emission initiating in the $7A_{1g}(^1S_0)$ level; however, the results of the electronic structure of this highly symmetric crystal are used as a model system to try to understand why the second step in photon cascade emission is not efficient in the low-symmetry $\text{YF}_3:\text{U}^{4+}$ crystal.

ACKNOWLEDGMENTS

This research was supported in part by Ministerio de Educación y Ciencia, Spain under Contract No. BQU2002-01316. One of the authors (B.O.) acknowledges an FPI fellowship from Ministerio de Ciencia y Tecnología, Spain.

- ¹S. V. Godbole, A. G. Page, Sangeeta, S. C. Sabharwal, J. Y. Gesland, and M. D. Sastry, *J. Lumin.* **93**, 213 (2001).
- ²Sangeeta, S. C. Sabharwal and J. Y. Gesland, *J. Lumin.* **93**, 167 (2001).
- ³N. Yu. Kirikova, M. Kirm, J. C. Krupa, V. N. Makhov, G. Zimmerer, and J. Y. Gesland, *J. Lumin.* **97**, 174 (2002).
- ⁴M. Kirm, J. C. Krupa, V. N. Makhov, E. Neodin, G. Zimmerer, and J. Y. Gesland, *J. Lumin.* **104**, 85 (2003).
- ⁵B. R. Judd, *Phys. Rev. Lett.* **39**, 242 (1977).
- ⁶C. A. Morrison, *J. Chem. Phys.* **72**, 1001 (1980).
- ⁷M. Bettinelli and R. Moncorgé, *J. Lumin.* **92**, 287 (2001).
- ⁸J. L. Ryan, J. M. Cleveland, and G. H. Bryan, *Inorg. Chem.* **13**, 214 (1974).
- ⁹W. Wagner, N. Edelstein, B. Whittaker, and D. Brown, *Inorg. Chem.* **16**, 1021 (1977).
- ¹⁰L. Seijo and Z. Barandiarán, *J. Chem. Phys.* **118**, 5335 (2003).
- ¹¹Z. Barandiarán and L. Seijo, *J. Chem. Phys.* **118**, 7439 (2003).
- ¹²R.-L. Chien, J. M. Berg, D. S. McClure, P. Rabinowitz, and B. N. Perry, *J. Chem. Phys.* **84**, 4168 (1986).
- ¹³M. Wermuth and H. U. Güdel, *J. Lumin.* **87**, 1014 (2000).
- ¹⁴C. Campochiaro, D. S. McClure, and H. H. Patterson, *Inorg. Chem.* **31**, 2809 (1992).
- ¹⁵L. H. Ahrens, *Geochim. Cosmochim. Acta* **2**, 155 (1952).
- ¹⁶R. D. Shannon and C. T. Prewitt, *Acta Crystallogr., Sect. B: Struct. Crystallogr. Cryst. Chem.* **25**, 925 (1969).
- ¹⁷B. Ordejón, L. Seijo, Z. Barandiarán, and M. Karbowiak (unpublished).
- ¹⁸Z. Barandiarán and L. Seijo, *J. Chem. Phys.* **89**, 5739 (1988).
- ¹⁹L. Seijo and Z. Barandiarán, in *Computational Chemistry: Reviews of Current Trends*, edited by J. Leszczyński (World Scientific, Singapore, 1999), Vol. 4, p. 55.
- ²⁰Z. Barandiarán and L. Seijo, *J. Chem. Phys.* **119**, 3785 (2003).
- ²¹L. Seijo, Z. Barandiarán, and D. S. McClure, *Int. J. Quantum Chem.* **80**, 623 (2000).
- ²²R. W. G. Wyckoff, *Crystal Structures* (Wiley, New York, 1968).
- ²³L. Seijo, Z. Barandiarán, and B. Ordejón, *Mol. Phys.* **101**, 73 (2003).
- ²⁴Z. Barandiarán and L. Seijo, *Can. J. Chem.* **70**, 409 (1992).
- ²⁵T. H. Dunning and P. J. Hay, in *Modern Theoretical Chemistry*, edited by H. F. Schaefer III (Plenum, New York, 1977).
- ²⁶J. Andzelm, M. Klobukowski, E. Radzio-Andzelm, Y. Sakai, and H. Tatewaki, *Gaussian Basis Sets for Molecular Calculations*, edited by S. Huzinaga (Elsevier, Amsterdam, 1984).
- ²⁷B. O. Roos, P. R. Taylor, and P. E. M. Siegbahn, *Chem. Phys.* **48**, 157 (1980); P. E. M. Siegbahn, A. Heiberg, J. Almlöf, and B. O. Roos, *J. Chem. Phys.* **74**, 2384 (1981); P. Siegbahn, A. Heiberg, B. Roos, and B. Levy, *Phys. Scr.* **21**, 323 (1980).
- ²⁸L. Seijo, *J. Chem. Phys.* **102**, 8078 (1995).
- ²⁹K. Andersson, P.-Å. Malmqvist, B. O. Roos, A. J. Sadlej, and K. Wolinski, *J. Phys. Chem.* **94**, 5483 (1990).
- ³⁰K. Andersson, P.-Å. Malmqvist, and B. O. Roos, *J. Chem. Phys.* **96**, 1218 (1992).
- ³¹J. Finley, P.-Å. Malmqvist, B. O. Roos and L. Serrano-Andrés, *Chem. Phys. Lett.* **288**, 299 (1998).
- ³²A. Zaitsevskii and J. P. Malrieu, *Chem. Phys. Lett.* **223**, 597 (1995).
- ³³R. Llugar, M. Casarrubios, Z. Barandiarán, and L. Seijo, *J. Chem. Phys.* **105**, 5321 (1996).
- ³⁴L. Seijo and Z. Barandiarán, *J. Chem. Phys.* **118**, 1921 (2003).
- ³⁵G. Karlström, R. Lindh, P. A. Malmqvist *et al.*, *Comput. Mater. Sci.* **28**, 22 (2003).
- ³⁶R. M. Pitzer, COLUMBUS suite of programs (ARGOS, CNVRT, SCFPO, LSTRN, CGDBG, and CIDBG); see A. H. H. Chang and R. M. Pitzer, *J. Am. Chem. Soc.* **111**, 2500 (1989), and references therein for a description. CNVRT and LSTRN have been adapted to handle AIMP integrals by L. Seijo. CIDBG has been modified for spin-free-state-shifted spin-orbit CI calculations by M. Casarrubios.
- ³⁷Detailed core and embedding AIMP data libraries in electronic format are available from the authors upon request or directly at the address <http://www.uam.es/quimica/aimp/Data/-AIMPLibs.html>. See also Ref. 35.

- ³⁸W. Xu, S. Dai, L. M. Toth, and J. R. Peterson, Chem. Phys. **193**, 339 (1995).
- ³⁹P. A. Tanner, J. Dexpert-Ghys, Z. W. Pei, and J. Lin, Chem. Phys. **215**, 125 (1997).
- ⁴⁰C. H. H. Van Deurzen, K. Rajnak, and J. G. Conway, J. Opt. Soc. Am. B **1**, 45 (1984).
- ⁴¹J.-F. Wyart, A. Raassen, P. Uylings, and Y. Joshi, Phys. Scr., T **47**, 59 (1993).
- ⁴²C. D. Flint and P. A. Tanner, Mol. Phys. **53**, 429 (1984).
- ⁴³C. D. Flint and P. A. Tanner, Mol. Phys. **53**, 437 (1984).
- ⁴⁴S. Kück, I. Sokólska, M. Henke, M. Döring, and T. Scheffler, J. Lumin. **102**, 176 (2003).